INTERNATIONAL ATOMIC ENERGY AGENCY
UNITED NATIONS EDUCATIONAL, SCIENTIFIC AND CULTURAL ORGANIZATION
INTERNATIONAL CENTRE FOR THEORETICAL PHYSICS
I.C.T.P., P.O. BOX 586, 34100 TRIESTE, ITALY. CABLE CENTRATOM TRIESTE

SMR.764 - 9

RESEARCH WORKSHOP ON CONDENSED MATTER PHYSICS
13 JUNE - 19 AUGUST 1994

MINIWORKSHOP ON "NONLINEAR TIME SERIES ANALYSIS" 8 - 12 AUGUST 1994

"Geometric Analysis of Time Series"

M. LEFRANC
Laboratoire de Spectroscopie Hertzienne
URA CNRS 249
Universite de Lille I
F-59655 Villeneuve d'Ascq
France

These are preliminary lecture notes intended only for distribution to participants

accepted for publication in Phys Rev Lett.

Combining Topological Analysis and Symbolic Dynamics to describe a Strange Attractor and its Crises

M. Lefranc,[1] P. Glorieux,[1] F. Papoff,[2] F. Molesti,[3] and E. Arimondo [3]
[1] *Laboratoire de Spectroscopie Hertzienne, URA CNRS 249, Université de Lille I, F-59655 Villeneuve d'Ascq, France.*
[2] *Physics Department, University of Strathclyde, 107 Rottenrow, Glasgow, G4 ONG, United Kingdom.*
[3] *Dipartimento di Fisica, Piazza Torricelli 2, 56126 Pisa, Italy.*
(July 27, 1993. Revised July 22, 1994)

We show how to use topological analysis to construct from experimental data a symbolic coding of a chaotic attractor. Time series data from a chaotic CO_2 laser with modulated losses operating within parameter regions corresponding to attractor crises have been analyzed. A procedure for determining a generating partition from the data is presented, and the connection between crises and a symbolic description of the dynamics is determined.

PACS numbers:05.45.+b, 42.50.Ne, 42.55.Lt

Unstable periodic orbits have been recognized as a major tool in characterizing low-dimensional chaotic behavior, particularly because they can be extracted from experimental time series [1]. An analysis of strange attractors proposed by Mindlin *et al.* [2] proceeds by determining the topological organization of these orbits, and has been successfully applied to a few experimental systems [3–5], including the laser with modulated losses (LML) used in the experiments reported below [6].

Key to this approach is the fact that, for an attractor embedded in a three-dimensional (3D) phase space, topological invariants, such as linking numbers or knot polynomials [7], may be used to determine in which way its periodic orbits are knotted and linked with each other. Moreover, there is a one-to-one correspondence between unstable periodic orbits of a 3D hyperbolic chaotic flow and periodic orbits carried by a 2D branched manifold, the "template" (or "knot-holder") [8], each periodic orbit of the flow having the same invariants as the associated template orbit. Experimental strange attractors are generally not hyperbolic, but the existing orbits are organized as in the hyperbolic limit as they cannot intersect on their whole domain of existence.

Coding trajectories as sequences of symbols (symbolic dynamics), is another powerful approach used to classify chaotic evolution and is intimately connected to topological analysis [8]. Methods to construct symbolic codings for 2D maps, including Poincaré maps of 3D flows, have been proposed [9], but their application to experimental systems seems difficult. This explains why topological analysis has been applied so far only to experimental investigations where symbolic coding could be obtained by means of 1D first return maps [3–6].

In this Letter, we apply the topological and symbolic dynamics approaches to cases where methods based on a 1D first return map method cannot be used. As the modulation amplitude is increased, the LML exhibits a series of crises [10–12] which widen or destroy the attractor [13]. Beyond the first crisis, no well-defined 1D map can be found, and thus there is no simple symbolic coding. However, this does not preclude the existence of a well-defined symbolic coding: one objective of this Letter is to present a method of constructing such a coding from the experimental data. We also want to show that, with or without a symbolic coding, important information can be extracted from the topological invariants of the unstable periodic orbits.

To check if the topological structure of the attractor is preserved in the crises, we have followed a self-consistent approach first used by Solari and Gilmore in their analysis of a theoretical model [14]. We have matched invariants of experimental periodic orbits to those of orbits with the same period belonging to the previously determined pre-crisis template [6], the Smale's horseshoe (SH) template with zero global torsion [8].

Identification of topologically allowed symbolic names for the detected periodic orbits has revealed that the observed crises are associated with the appearance of particular symbol sequences in the symbolic dynamics. If periodic orbits are classified on the basis of these sequences, we find that a crisis occurs when all orbits in a given class have been created. Furthermore, the topological identification of periodic orbits, with only a small part needed to determine the template, has allowed us, to construct a symbolic coding for the experimental data by determining an approximate generating partition. This allowed us to study the order of appearance of periodic orbits with specified names when parameters change, and to compare this order with the "kneading order" [8] (the latter classifies periodic orbits of unimodal maps of the interval with respect to their symbolic name, and predicts in which order they are generically created in such maps).

This approach, combining topology and symbolic dynamical concepts, represents a general and very powerful method to analyze experimental data without the restriction of the 1D first return map, and to define a more precise generating partition than that found empirically in Refs. [15,16].

The experimental setup consists of a waveguide CO_2 laser with intracavity losses modulated at a frequency of

382.5 kHz. This system is well-known to display chaotic behavior [10–12,17]. Rather than the output intensity I of the laser, we have recorded $X = \log I$ which was recently shown to be a more efficient variable to characterize chaotic regimes [18]. Fig. 1 displays a segment of a typical time series. For various values of modulation amplitude and laser frequency detuning, we have recorded from 25 to 100 files, containing each 32000 8-bit samples, at a sampling rate of approximatively 65 samples per period.

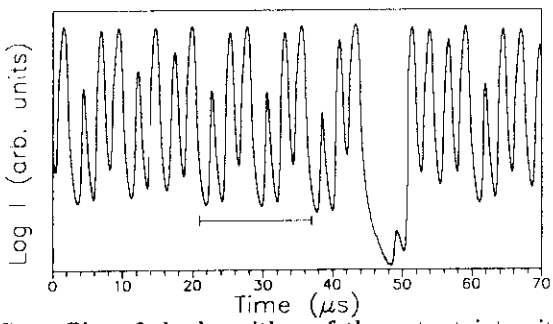

FIG. 1. Plot of the logarithm of the output intensity vs. time. The underlined segment shadows a period $3T$ orbit.

Periods of unstable orbits are integer multiples of the modulation period T. A segment of the time series $X(t)$ where $|X(t+nT) - X(t)| < \epsilon$ for $t_0 < t < t_0 + nT$ indicates that the system trajectory in phase space shadows a period nT orbit, and may be used as an approximation of this orbit. Fig. 1 shows such a burst of periodic behavior. We have only kept segments for which ϵ was smaller than 4 % of the maximum amplitude of $X(t)$, but for most extracted orbits, representative segments with ϵ of the order of the digitizing noise (i.e. 1 %) have been detected, thanks to the very low internal noise of the laser used in the experiments. For each set of parameters, we have typically extracted from 20 to 38 orbits with a period lower than or equal to $13T$, with up to 304 periodic points in a Poincaré section.

If periodic orbits are embedded in a phase space with coordinates $(X(t), dX(t)/dt, \phi)$, where $\phi = t/T \ mod \ 1$ is the phase of the forcing term, their regular isotopy invariants can easily be obtained by plotting the corresponding time series segment versus ϕ (Fig. 2) [6], which gives a representation of the orbit as a braid on n strands [7]. For each periodic orbit, the following invariants were determined: self-relative rotation rates and torsion (the latter characterizing the rotation of nearby trajectories around the orbit), as well as relative rotation rates and linking numbers with other orbits [3,14].

Template determination is most easily performed when a symbolic coding of trajectories on the attractor is already available: the template is constructed so that attractor and template orbits with the same name have identical invariants. Let us recall that if a different symbol is assigned to each branch of a template, this provides

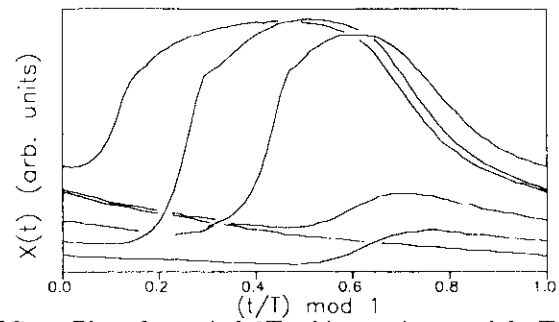

FIG. 2. Plot of a period $6T$ orbit vs. time modulo T. Under- and overcrossings are determined as explained in ref. [6].

for each periodic orbit on it a symbolic name listing successively visited branches. We will call thereafter x (y) the orientation-preserving (-reversing) branch of the SH template.

Once a coding can be obtained from a partition of a Poincaré section, with a different symbol for each of its members, each trajectory may be coded with the symbols associated to successive intersections with the section plane. A partition is generating (i.e. associates to each bi-infinite sequence a unique point in the section plane), only if each periodic orbit is given a unique symbolic name. While the existence of generating partitions for nonhyperbolic systems is not rigorously ascertained, there is numerical evidence that partitions can be constructed which are generating down to scales well below realistic experimental resolutions [9].

Determining experimentally such a partition is not straightforward, except when an almost 1D first return map can be constructed, with a symbol assigned to each monotonic part of the map. For low modulation amplitudes, we could always find such a map and Fig. 3(a) shows a Poincaré section obtained in this case. For these parameters, the template is the SH template [6].

At higher amplitudes, after an interior crisis [13,10–12] in which the attractor suddenly widens after colliding with the xyy ($\equiv xy^2$) $3T$ unstable orbit, the first return diagram of $X(t+T)$ versus $X(t)$ associated to any Poincaré section, such as the one in Fig. 3(b), is multivalued and thus not the graph of a 1D map. In this case, it is not even clear whether new symbols should be used, though the method of sweeping Poincaré sections (see e.g. Ref [6]) apparently indicates that the stretching and folding mechanisms remain unchanged. Thus we have only the topological invariants from which to extract the symbolic information.

Invariants of single orbits show remarkable robustness with respect to experimental uncertainties. When the signal to noise ratio is high, as here, very few (typically 2–3 %) measured linking numbers of close orbits may differ from their actual value due to spurious crossings [6]. These discrepancies are however easily detected, being inconsistent with other measured invariants; unless dis-

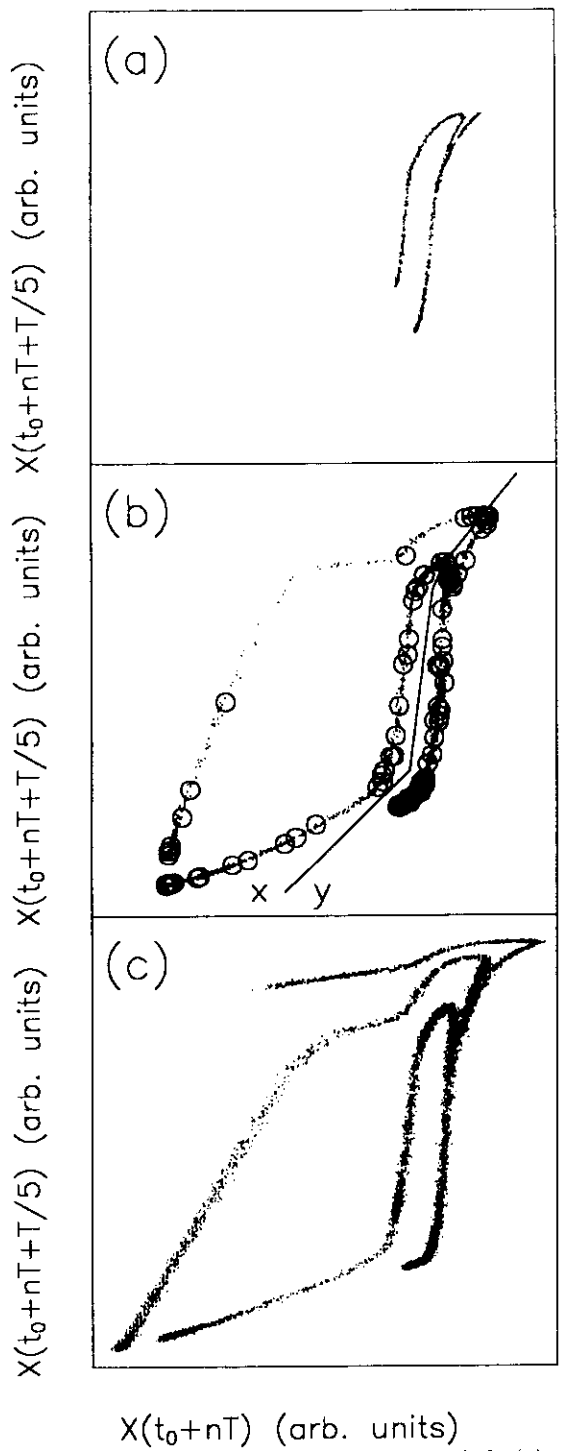

FIG. 3. Poincaré sections of attractors recorded: (a) at low modulation amplitudes (contains only C_2 orbits), (b) after collision with the $3T$ orbit xy^2 (contains C_2 and C_3 orbits, circles are intersections of periodic orbits with the section plane, the solid line is the boundary of an approximate generating partition), (c) after collision with the $4T$ x^2y^2 orbit (contains C_2, C_3 and C_4 orbits)

carded, they prevent any template from fitting the data. We found that the SH template is the simplest template compatible with data recorded beyond the crisis.

For a certain number of periodic orbits, including most of low period ones, invariants are genuine fingerprints: they correspond to a unique SH orbit, and only one symbolic name may be assigned to these orbits. More generally, determining all sets of SH orbits with invariants identical to experimental ones left us with only a few possible symbolic names for each periodic orbit.

Although symbolic names of all orbits are not fully determined in this way, a remarkable feature nevertheless emerges: defining a C_n orbit as having a name containing the sequence x^{n-1}, but not the x^n one (e.g. the name of a C_2 orbit only contains isolated x's), every orbit visiting the pre- (post-) crisis part of the attractor can only be a C_2 (C_3) orbit. The crisis thus coincides with the appearance of the previously forbidden sequence x^2 in the symbolic dynamics. This simple rule has also been reported for a NMR oscillator [16], but it should be stressed that it is obtained here from merely computing topological invariants, without relying on any partition. Furthermore, we have found this rule to be part of a pattern, as shown by the following scenario observed as the modulation amplitude was increased.

The attractor of Fig. 3(b) first collides with the unstable $4T$ orbit x^2y^2 (identified by its invariants), and the system switches to the stable $4T$ orbit x^3y, which gives birth through period-doublings to a four-piece chaotic attractor. This attractor experiences then an interior crisis involving the x^2y^2 orbit again, after which the Poincaré section in Fig. 3(c) has been recorded. The corresponding attractor next collides with the x^3y^2 orbit, and motion settles down on the stable orbit x^4y.

All these crises are thus due to collisions with the $x^{n-1}y^2$ orbits, and the sequences x^n appear just after such collisions, at least, as observed here, for $n = 2$, 3 and 4. Note that the $x^{n-1}y^2$ and x^ny orbits ($n \geq 2$) are the only period $n+1$ unknotted SH orbits. Moreover, just before the collision with the xy^2 orbit, we have unambiguously detected the $13T$ orbit $(xy^2)^4y$, which is "quasi-one-dimensional" (qod): its presence implies the existence of all periodic orbits preceding it in the kneading order [19]. This proves the presence of all C_2 orbits up to period $13T$, and of almost all higher order C_2 orbits: the collision with the xy^2 orbit very likely occurs just after all C_2 orbits have been created. Similarly, the collision with the x^2y^2 orbit should occur when all C_3 orbits have been created, as shown by the presence of the $(x^2y^2)^3y$ qod orbit in files recorded just before this collision. Thus, there appears to be a deep connection between the observed crises and the spectrum of periodic orbits.

Selecting periodic orbits with an unambiguous name, we have constructed a partition of the section plane in Fig. 3(b), so that it gives to each periodic orbit its topo-

logical symbolic name. This partition is defined by a list of reference points, each associated to a symbol; intersections of trajectories with the section plane are coded with the symbol assigned to the closest reference point. To get a partition as simple as possible, we proceeded through successive refinements. First, $1T$ and $2T$ periodic points y and xy were the only reference points. Then, for each periodic orbit from low-period to high-period ones, the following steps were carried out: (i) the cyclic permutation of the topological symbolic name least differing from the name given by the partition was first determined, (ii) periodic points for which a discrepancy remained were then added to the reference list to update the partition. In this way, large-scale features are determined from low period orbits, while small-scale details of the partition are extracted from high period ones.

The boundary of the approximate partition so obtained usually can be localized within a region small enough to code points not in its vicinity without ambiguity. We have thus used this partition to identify substrings of symbolic names of not yet identified periodic orbits, and discarded symbolic names not containing these substrings. Alternatively checking topological consistency and refining the accuracy of the partition with newly identified orbits, we finally determined for each orbit a unique symbolic name, the resulting partition is shown in Fig. 3(b). Note that, whereas detected orbits do not uniformly cover the attractor, they are found in abundance near the boundary of the partition, which makes the precision of the latter of the order of the experimental resolution. Furthermore the partition is seen to pass near but not exactly through the most apparent folds of the Poincaré section, showing that naively connecting these latter would not yield a correct solution.

Data files recorded as the modulation amplitude was increased contain an increasing number of unstable periodic orbits. Before the first crisis, we have observed that periodic orbits appear in an order corresponding to the kneading order for C_2 orbits, at least up to period $8T$. Similarly, between the collisions with the xy^2 and x^2y^2 orbits, kneading order governs the order of appearance of lowest periodic orbits. Note that in this case, some symbolic names have been obtained by means of partitions as described above: the agreement with the kneading order seems to indicate that these partitions yield sensible symbolic codings.

In unimodal maps of the interval such as the logistic map, C_n orbits appear only when all C_{n-1} orbits have been created. This is not true in the LML, which is known to exhibit multistability [17,10–12,14]: C_3 or C_4 orbits may coexist with a C_5 attractor, and thus the kneading order governs the order of appearance of periodic orbits only within each class C_n of orbits. As noted in Ref. [13], multistability and the subsequent crises can occur even in highly dissipative systems, such as the LML in our case, for which correlation dimension estimates near 2.1 have been obtained [18], while the relation between multistability and dissipativity has been addressed by Arecchi *et al.* [11] in the context of the LML. From the above symbolic dynamical analysis, we see that these phenomena are very much controlled by the topological organization of the unstable periodic orbits, and certainly deserve further study through topological methods.

In conclusion, we have determined the template for the LML in parameter regions where there was no simple symbolic coding. The topological information extracted from unstable periodic orbits allowed us to very simply characterize the observed crises in terms of symbolic dynamics. The fact that their organization can be analyzed entirely by symbolic dynamics implies that the features reported here should hold for many horseshoe-like chaotic systems. We have also constructed an approximate symbolic coding for the experimental data from the topological information. The methods presented here may be improved, yet we believe they already clearly illustrate how powerful topology methods can unfold chaotic complexity in experimental systems.

We are very much indebted to R. Gilmore for useful discussions and a careful reading of the manuscript. We also thank N. B. Tufillaro and T. D. Hall for useful advice and communicating their work before publication.

[1] D. Auerbach, P. Cvitanović, J.-P. Eckmann, G. H. Gunaratne, and I. Procaccia, Phys. Rev. Lett. **58**, 2387 (1987).

[2] G. B. Mindlin, X.-J. Hou, H. G. Solari, R. Gilmore, and N. B. Tufillaro, Phys. Rev. Lett. **64**, 2350 (1990).

[3] G. B. Mindlin, H. G. Solari, M. A. Natiello, R. Gilmore, and X.-J. Hou, J. Nonlinear Sci. **1**, 147 (1991).

[4] N. B. Tufillaro, R. Holzner, L. Flepp, M. F. E. Brun, and R. Badii, Phys. Rev. A **44**, R4786 (1991).

[5] F. Papoff, A. Fioretti, E. Arimondo, G. B. Mindlin, H. G. Solari, and R. Gilmore, Phys. Rev. Lett. **68**, 1128 (1992).

[6] M. Lefranc and P. Glorieux, Int. J. Bifurcation and Chaos **3**, 643 (1993).

[7] L. H. Kaufmann, *Knots and Physics* (World Scientific, Singapore, 1991).

[8] P. Holmes, in *New Directions in Dynamical Systems*, edited by T. Bedford and J. Swift (Cambridge University Press, Cambridge, 1988), p. 150.

[9] P. Grassberger, H. Kantz, and U. Moenig, J. Phys. A **22**, 5217 (1989). P. Cvitanović, G. H. Gunaratne, and I. Procaccia, Phys. Rev. A **38**, 1503 (1988). F. Giovannini and A. Politi, J. Phys. A **24**, 1837 (1991).

[10] D. Dangoisse, D. Hennequin, and P. Glorieux, Phys. Rev. Lett. **57**, 2657 (1986).

[11] R. Meucci, A. Poggi, F. T. Arecchi, and J. R. Tredicce, Opt. Commun. **65**, 151 (1987).

[12] H. G. Solari, E. Eschenazi, R. Gilmore, and J. R. Tredicce, Opt. Commun. **64**, 49 (1987).

[13] C. Grebogi, E. Ott, and J. A. Yorke, Physica **7D**, 181 (1983).

[14] H. G. Solari and R. Gilmore, Phys. Rev. A **37**, 3096 (1988).

[15] L. Flepp, R. Holzner, E. Brun, M. Finardi, and R. Badii, Phys. Rev. Lett. **67**, 2244 (1991).
[16] M. Finardi, L. Flepp, J. Parisi, R. Holzner, R. Badii, and E. Brun, Phys. Rev. Lett. **68**, 1989 (1992).
[17] F. T. Arecchi, R. Meucci, G. P. Puccioni, and J. R. Tredicce, Phys. Rev. Lett. **49**, 1217 (1982). T. Midavaine, D. Dangoisse, and P. Glorieux, *ibid.* **55**, 1989 (1985). J. R. Tredicce, F. T. Arecchi, G. P. Puccioni, A. Poggi, and W. Gadomski, Phys. Rev. A **34**, 2073 (1986). D. Hennequin, D. Dangoisse, and P. Glorieux, *ibid.* **36**, 4775 (1987).
[18] M. Lefranc, D. Hennequin, and P. Glorieux, Phys. Lett. A **163**, 269 (1992).
[19] T. D. Hall, Phys. Rev. Lett. **71**, 58 (1993).

International Journal of Bifurcation and Chaos, Vol. 3, No. 3 (1993) 643–650

TOPOLOGICAL ANALYSIS OF CHAOTIC SIGNALS FROM A CO_2 LASER WITH MODULATED LOSSES

MARC LEFRANC and PIERRE GLORIEUX
Laboratoire de Spectroscopie Hertzienne (Unité de Recherche associée au CNRS), UFR de Physique, Université de Lille I, F-59655 Villeneuve d'Ascq, France.

Received September 20, 1992; Revised October 30, 1992

Unstable periodic orbits have been extracted from chaotic time series coming from a CO_2 laser with modulated losses. Topological analysis of their organization reveals that chaos in this laser occurs through the formation of a Smale's horseshoe.

A topological method has recently been proposed to analyse experimental time series from low-dimensional chaotic systems [Mindlin *et al.*, 1990]. It relies on the identification of unstable periodic orbits embedded in the strange attractor associated with chaotic behavior, and on the analysis of their topological organization. Indeed, periodic orbits of dynamical systems are closed curves in phase space, and the uniqueness theorem [Guckenheimer & Holmes, 1983] precludes that they intersect each other as a control parameter is varied. When a strange attractor can be embedded in a three-dimensional phase space, topological invariants from knot theory [Kauffman, 1987] may thus be used to determine in which way its unstable periodic orbits are knotted and linked together. The global organization of periodic orbits can then be characterized by a two-dimensional branched manifold, the template (or "knot holder") [Birman & Williams, 1983] (see also [Holmes, 1988; Tufillaro *et al.*, 1992]) in which they can be embedded while preserving their topological invariants. The structure of the template is described with a small set of integers which depend only on the properties of orbits of lowest period, and can be used to classify attractors.

This analysis has been successfully applied to experimental time-series data from the Belousov-Zhabotinskii reaction [Mindlin *et al.*, 1991], from a laser containing a saturable absorber [Papoff *et al.*, 1992] and from an NMR oscillator [Tufillaro *et al.*, 1991]. We report here the result of such an analysis in the case of the CO_2 laser with sinusoidally modulated losses.

This laser is known to reach chaos through a cascade of period-doubling bifurcations and has been the subject of intense investigations [Arecchi *et al.*, 1982; Midavaine *et al.*, 1985; Dangoisse *et al.*, 1987]. The various control parameters include cavity frequency detuning and the amplitude of the external driving, the frequency of which being equal to 382.5 kHz in our experiments. Experimental data analysed here have been obtained from the laser as described by Lepers *et al.* [1991]. Because of the high stability of the laser, files may be successively stored and sets of 25 to 100 files of 32000 samples have been analysed for each setting of the control parameters.

Correlation dimension analyses using the Grassberger-Procaccia algorithm [Grassberger & Procaccia, 1983] have been made on signals coming from this laser operated in the chaotic regime. They have shown that the reliability of dimension estimates is greatly improved when time series of the logarithm of the laser output intensity, rather than of the intensity $I(t)$ itself as in previous analyses, is used

PACS numbers: 05.45.+b, 42.50.Lc, 42.55.-f

to reconstruct an experimental strange attractor through the time delay method [Lefranc *et al.*, 1992]. This occurs because typical time series display long sequences of very weak intensity, resulting in a very large inhomogeneity of reconstructed strange attractors. It must be noted that because of the particular nature of the laser equations, Log I appears as a natural variable of the dynamical system [Oppo *et al.*, 1989]. Similarly, topological analysis using intensity is made meaningless by the uncertainties of the relative positions of trajectories in the near zero intensity region. The results reported here have therefore been obtained from time series of $\mathrm{Log}(I + I_0)$, where I_0 is a very small constant which can be adjusted in the logarithmic amplifier used for signal processing. This procedure was allowed by the high signal-to-noise ratio achieved in this laser, limited practically by the resolution (8 bits) of the transient digitizer used in these experiments.

Let us now describe the procedure of the analysis. First, unstable periodic orbits are extracted from time-series data by searching for close returns [Mindlin *et al.*, 1991]. The fact that our system is periodically driven simplifies this step, since periodic orbits have periods which are multiples of the modulation period $T = 2\pi/\omega$. A segment of the time series $X(t)$ where $|X(t) - X(t + nT)| < \varepsilon$ for $t_0 < t < t_0 + nT$ indicates the shadowing of a period nT orbit by the trajectory of the system on the attractor, and can be used as an approximation to this orbit. In our analysis, ε was chosen to be equal to $0.04 \times (X_{\max} - X_{\min})$. Examples of such segments are shown in Fig. 1. The fact that the period T orbit on first row is shadowed very closely during several periods of modulation is an indication that the internal dynamics of our laser is very little perturbed by noise (similar sequences lasting up to 14 periods have been extracted). This allowed us to extract high order periodic orbits up to period $17T$. Note the peculiar case of the second row, where after a few cycles near a period $3T$ orbit the system enters directly the vicinity of a period $2T$ orbit. It should be stressed that a time series with strong recurrence properties has almost certainly a low-dimensional deterministic origin, as such bursts of almost periodic behavior are extremely unlikely in stochastic or high-dimensional systems.

Second, periodic orbits must be embedded in a three-dimensional phase space. Taking advantage of the particular nature of periodically driven systems, we used $\{X(t),\ X(t + \tau),\ \phi\}$ or $\{X(t),\ dX(t)/dt,\ \phi\}$ embeddings, where τ is a time delay and $\phi = \omega t \bmod 2\pi$ is the phase of the external modulation. We found that these two phase spaces led to consistent results, provided that τ be small enough (i.e., smaller than $T/4$ in the worst case). An experimental strange attractor and the extracted unstable periodic orbits are displayed in Figs. 2(a) and 2(b) respectively, using the first kind of embedding. These two figures illustrate well the fact that the essential features of the dynamics can be obtained from the study of unstable periodic orbits. Note that $\{X(t),\ dX(t)/dt,\ \phi\}$ is the natural phase space of the system, as the free CO_2 laser is well described by two first-order ordinary differential equations (see, for example, Dangoisse *et al.*, [1987] or Oppo *et al.* [1989]).

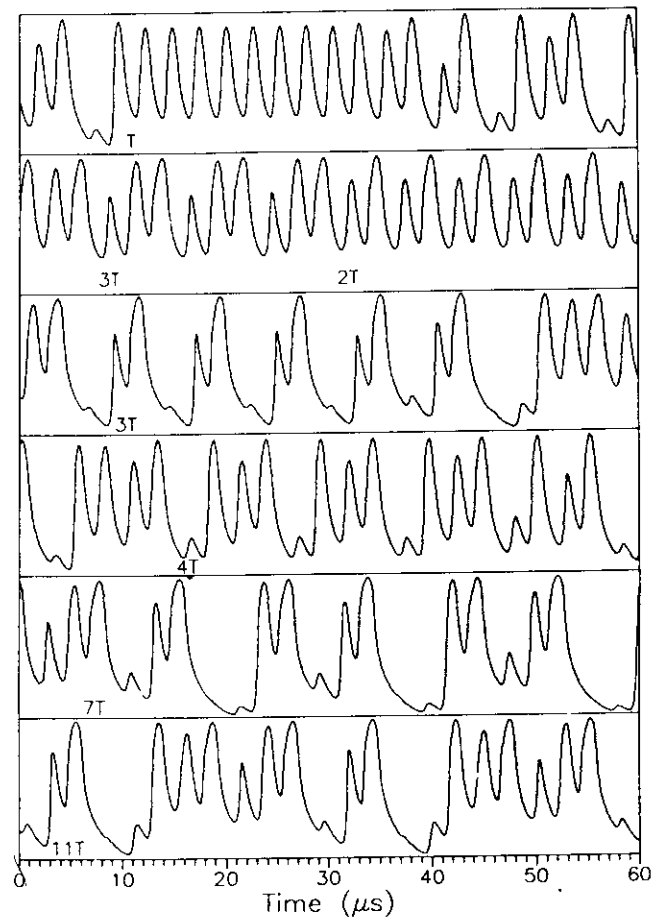

Fig. 1. Examples of time-series segments which closely follow unstable periodic orbits. Periods of these orbits are indicated at the beginning of segments.

More conveniently than in 3D phase space, the topological structure of periodic orbits can be analyzed by plotting the corresponding time-series seg-

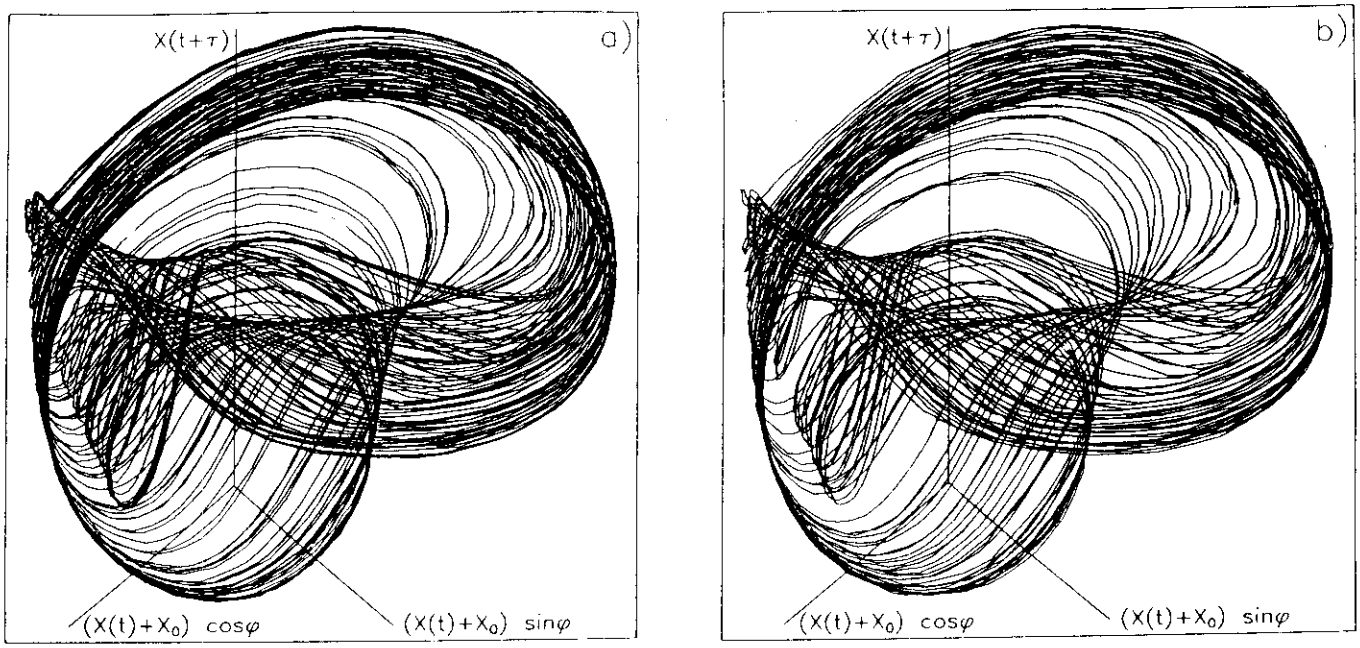

Fig. 2. (a) Experimental strange attractor reconstructed using an $\{X(t), X(t+\tau), \phi\}$ phase space with $\tau = T/4$. (b) Some unstable periodic orbits embedded in this attractor and extracted from the time series.

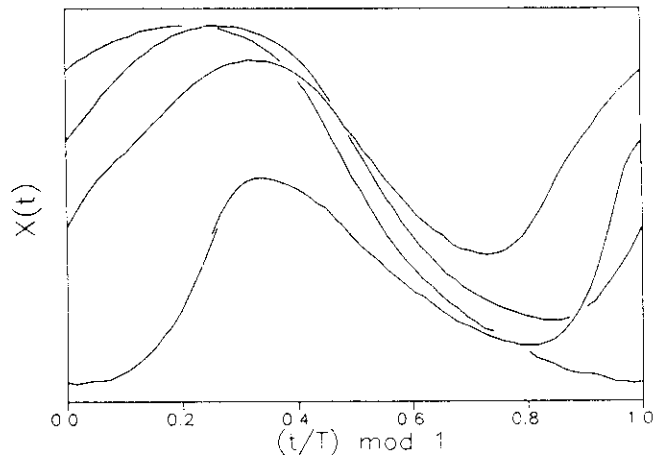

Fig. 3. Plot of a time-series segment corresponding to a period $4T$ orbit versus time modulo T.

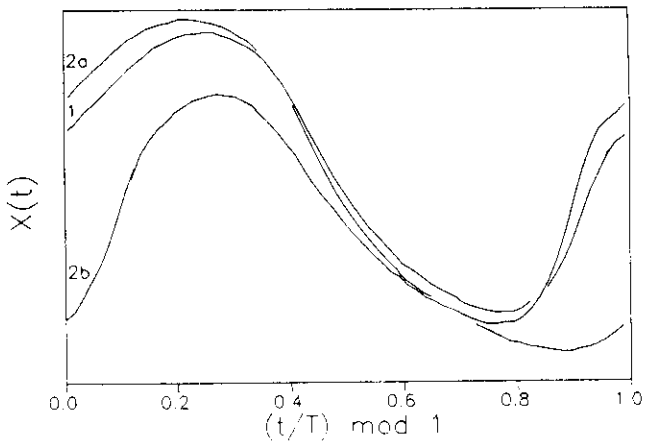

Fig. 4. Plot of time series segments to period T (strand 1) and $2T$ (strands 2a and 2b) orbits versus time modulo T.

ments versus time modulo T. Periodic orbits are represented in this way as braids on n strands [Birman, 1975], provided we determine for each crossing of two strands which one crosses over the other. This is straightforward if a $\{X(t), dX(t)/dt, \phi\}$ phase space is implicitly used. Indeed, whenever two strands cross, the one with a lower value of $X(t)$ before the crossing corresponds to a higher value of $dX(t)/dt$ (which is the coordinate perpendicular to the plot) and therefore passes over the other. This implies that only positive braids can be obtained. A braid on four strands representing a $4T$ orbit is shown in Fig. 3, where over- and undercrossings have been indicated for clarity, following this convention. Plotting together a period nT orbit and a period mT orbit gives in the same way a braid on $n+m$ strands, as in Fig. 4, where $1T$ and $2T$ orbits have been plotted.

Several invariants can be computed from the structure of the braid. They include linking numbers and relative rotation rates [Solari & Gilmore, 1988; Tufillaro *et al.*, 1990] for pairs of orbits, and self-relative rotation rates and knot polynomials [Kauffman, 1987] for single orbits. For example, the braid of Fig. 3 has self relative rotation rates equal to 0, 1/4, $(1/2)^2$ and is a representation of a trefoil knot with Conway polynomial $\nabla = 1 + z^2$. The linking number of the period 1 and period 2 orbits shown in Fig. 4 is 1, since they cross each other twice, and their relative rotation rate is 1/2. This information characterizes the topological organization of periodic orbits.

The results reported below have been obtained for chaotic regimes observed between the inverse period-doubling cascade of the $1T$ orbit and a crisis where the chaotic attractor collides with an unstable $3T$ orbit. In this region of parameter space, it has always been possible to find a Poincaré section of constant phase with a return map well approximated by a unimodal 1D map $X(t_0 + (n+1)T) = f(X(t_0+nT))$. The existence of such a map allowed us to assign a symbolic itinerary to each extracted periodic orbit, by labeling each of its intersections with the section plane "x" or "y", depending on whether the orientation-preserving or orientation-reversing branch of the first return map was visited. This procedure was also used in other topological investigations of chaotic systems [Mindlin *et al.*, 1991; Tufillaro *et al.*, 1991; Papoff *et al.*, 1992].

To illustrate this, Fig. 5 shows a 1D first return map obtained just before the crisis occurs, with points corresponding to a $7T$ periodic orbit. From the order in which they are successively visited, one can read that the symbolic itinerary of this orbit is $xyxyxy^2$. The fact that two different extracted periodic orbits receive in this way different names indicates that this binary symbolic encoding is a good approximation to a generating partition.

It can then be checked that a template can be constructed, so that each experimental periodic orbit is associated with a unique orbit of the template, with the same symbolic name and identical topological invariants.

The topological properties of the three lowest order periodic orbits suffice to determine the structure of any two-branch template [Mindlin *et al.*, 1991]. For most of the files analysed in the parameter space region under study, these orbits were the y, xy, and xy^3, orbits, whereas $3T$ orbit xy^2 could be extracted from signals recorded in the vicinity of the crisis. Indeed, this orbit is located on the boundary of the basin of attraction of the chaotic attractor, and the collision of this orbit with the attractor is responsible for the occurrence of a crisis.

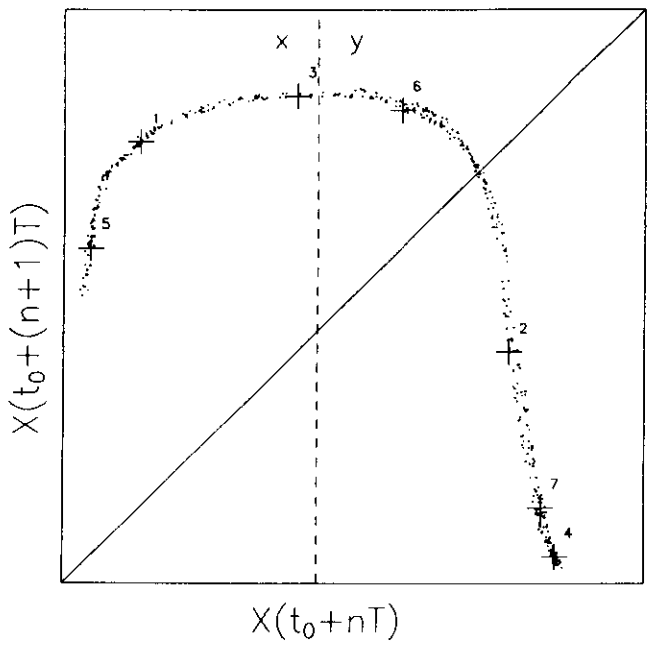

Fig. 5. 1D first return map on a Poincaré section of constant phase. Orientation-preserving and -reversing branches are labeled "x" and "y" respectively. Points corresponding to a $7T$ orbit have been plotted, from which the symbolic itinerary "$xyxyxy^2$" can be read.

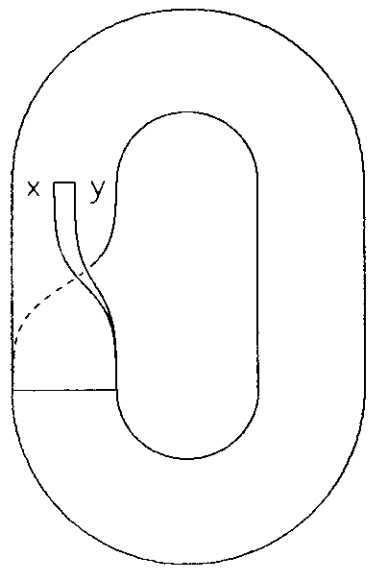

Fig. 6. The horseshoe template with zero global torsion. The "x" (respectively "y") branch is orientation-preserving (respectively-reversing).

Table 1. Relative rotation rates of extracted periodic orbits up to period $8T$. Values in square brackets have been obtained using the correction described in the text. Values in braces differ from those predicted by the horseshoe template.

Orbits		1	2	3	4	5a	5b	6a	6b
y	1	0							
xy	2	$\frac{1}{2}$	0, $\frac{1}{2}$						
xy^2	3	$\frac{1}{3}$	$\frac{1}{3}$	0, $(\frac{1}{3})^2$					
xy^3	4	$\frac{1}{2}$	$\frac{1}{2}$, $\frac{1}{4}$	$\frac{1}{3}$	0, $\frac{1}{4}$, $(\frac{1}{2})^2$				
xy^4	5a	$\frac{2}{5}$	$\frac{2}{5}$	$\frac{1}{3}$	$\frac{2}{5}$	0, $(\frac{2}{5})^4$			
$xyxy^2$	5b	$\frac{2}{5}$	$\frac{2}{5}$	$\frac{1}{3}$	$\frac{2}{5}$	$\frac{2}{5}$	0, $(\frac{2}{5})^4$		
$xyxy^3$	6a	$\frac{1}{2}$	$\frac{1}{2}$, $\frac{1}{3}$	$\frac{1}{3}$	$\frac{1}{2}$, $\frac{1}{3}$	$\frac{2}{5}$	$[\frac{2}{5}]$	0, $(\frac{1}{3})^2$, $(\frac{1}{2})^3$	
xy^5	6b	$\frac{1}{2}$	$\frac{1}{2}$, $\frac{1}{3}$	$\frac{1}{3}$	$\frac{1}{2}$, $\frac{1}{3}$	$[\frac{2}{5}]$	$\frac{2}{5}$	$\frac{1}{2}$, $\frac{1}{3}$	0, $(\frac{1}{3})^2$, $(\frac{1}{2})^3$
$xyxy^4$	7a	$\frac{3}{7}$	$\frac{3}{7}$	$\frac{1}{3}$	$\frac{3}{7}$	$\frac{2}{5}$	$[\frac{2}{5}]$	$[\frac{3}{7}]$	$[\frac{3}{7}]$
xy^6	7b	$\frac{3}{7}$	$\frac{3}{7}$	$\frac{1}{3}$	$\frac{3}{7}$	$\frac{2}{5}$	$[\frac{2}{5}]$	$\frac{3}{7}$	$[\frac{3}{7}]$
$(xy)^2xy^2$	7c	$\frac{3}{7}$	$\frac{5}{14}$	$\frac{1}{3}$	$[\frac{11}{28}]$	$\frac{2}{5}$	$\frac{13}{35}$	$\frac{8}{21}$	$\frac{17}{42}$
$(xy)^2xy^3$	8a	$\frac{1}{2}$	$\frac{1}{2}$, $\frac{1}{4}$	$\frac{1}{3}$	$\frac{1}{4}$, $[\frac{3}{8}]$, $(\frac{1}{2})^2$	$\frac{2}{5}$	$[\frac{2}{5}]$	$\frac{1}{3}$, $\frac{1}{2}$	$\frac{1}{2}$, $\frac{1}{3}$
xy^7	8b	$[\frac{1}{2}]$	$\frac{3}{8}$, $\frac{1}{2}$	$\frac{1}{3}$	$\frac{3}{8}$, $\frac{1}{2}$	$\frac{2}{5}$	$\frac{2}{5}$	$\frac{3}{8}$, $\frac{1}{2}$	$\{\frac{5}{12}\}$, $\frac{1}{2}$
$xyxy^5$	8c	$\frac{1}{2}$	$\frac{3}{8}$, $\frac{1}{2}$	$\frac{1}{3}$	$[\frac{3}{8}]$, $\frac{1}{2}$	$\frac{2}{5}$	$[\frac{2}{5}]$	$\{\frac{5}{12}\}$, $\frac{1}{2}$	$[\frac{3}{8}]$, $\frac{1}{2}$
xy^2xy^4	8d	$\frac{3}{8}$	$\frac{3}{8}$	$\frac{1}{3}$	$\frac{3}{8}$	$\frac{3}{8}$	$[\frac{3}{8}]$	$\frac{3}{8}$	$\frac{3}{8}$

Orbits		7a	7b	7c	8a	8b	8c	8d
$xyxy^4$	7a	0, $(\frac{3}{7})^6$						
xy^6	7b	$[\frac{3}{7}]$	0, $(\frac{3}{7})^6$					
$(xy)^2xy^2$	7c	$(\frac{3}{7})^5$, $(\frac{2}{7})^2$	$(\frac{3}{7})^6$, $(\frac{2}{7})$	0, $(\frac{2}{7})^2$, $(\frac{3}{7})^4$				
$(xy)^2xy^3$	8a	$[\frac{3}{7}]$	$\frac{3}{7}$	$\frac{3}{8}$	0, $\frac{3}{8}$, $(\frac{1}{4})^2$, $(\frac{1}{2})^4$			
xy^7	8b	$[\frac{3}{7}]$	$[\frac{3}{7}]$	$\frac{23}{56}$	$\frac{3}{8}$, $\frac{1}{2}$	0, $(\frac{3}{8})^3$, $(\frac{1}{2})^4$		
$xyxy^5$	8c	$\{\frac{23}{56}\}$	$\frac{3}{7}$	$[\frac{11}{28}]$	$\frac{3}{8}$, $\frac{1}{2}$	$\frac{3}{8}$, $\frac{1}{2}$	0, $(\frac{3}{8})^3$, $(\frac{1}{2})^4$	
xy^2xy^4	8d	$\frac{3}{8}$	$\frac{3}{8}$	$[\frac{3}{8}]$	$\frac{3}{8}$	$\frac{3}{8}$	$\frac{3}{8}$	0, $(\frac{3}{8})^7$

At each parameter value, the lowest order periodic orbits have been found to be knotted and linked as in the Smale's horseshoe template with zero global torsion [Holmes & Williams, 1985], which is shown in Fig. 6. Furthermore, it has been checked that invariants of higher order orbits were correctly predicted by this template, as is required to give definite evidence that its structure determines the global topological organization of the attractor.

As an example, we present results for a chaotic attractor about to collide the xy^2 orbit, as many periodic orbits could be extracted from the corresponding signals. The associated first return map is shown in Fig. 5.

The corresponding relative rotation rates of orbits up to period $8T$ are shown in Table 1. To compute them, the number of crossings of two strands of the braids was determined by looking for time intervals where the distance between them was smaller than some constant η. If the relative positions of the two strands at the beginning and at the end of such an interval were different, one crossing was counted. Choosing $\eta = 3\,b_0$, where b_0 is the least

Table 2. Self relative rotation rates of extracted periodic orbits from period $9T$ up to period $12T$.

Orbits		Self Relative Rotation Rates
$(xy)^3xy^2$	9a	$0, (\frac{1}{3})^4, (\frac{4}{9})^4$
xy^2xy^5	9b	$0, (\frac{1}{3})^4, (\frac{4}{9})^4$
$(xy)^2xy^4$	9c	$0, (\frac{1}{3})^2, (\frac{4}{9})^6$
xy^3xy^4	9d	$0, (\frac{1}{3})^2, (\frac{4}{9})^6$
$xyxy^2xy^4$	10a	$0, \frac{3}{10}, (\frac{2}{5})^8$
$xyxy^4xy^2$	10b	$0, \frac{3}{10}, (\frac{2}{5})^8$
$(xy)^4xy^2$	11a	$0, (\frac{3}{11})^2, (\frac{4}{11})^4, (\frac{5}{11})^4$
$xyxy^3xy^4$	11b	$0, (\frac{4}{11})^4, (\frac{5}{11})^6$
$xyxy^2xy^5$	11c	$0, (\frac{5}{11})^4, (\frac{4}{11})^6$
$xy(xy^2)^3$	11d	$0, (\frac{4}{11})^{10}$
$(xy)^2xy^4xy^2$	12a	$0, (\frac{1}{3})^4, (\frac{5}{12})^7$
xy^2xy^8	12b	$0, (\frac{1}{3})^2, (\frac{5}{12})^9$

significant bit of the digitizer (i.e., η is 1.2% of the maximum amplitude of the signal), prevents counting spurious crossings caused by digitizing noise or by imperfect shadowing of orbits.

However, there remained a few discrepancies, especially when dealing with orbits very close to each other. We observed that these errors occurred when two orbits were closer than η over more than a full period of modulation. It was possible in these cases to find long time intervals where no crossing was detected by the procedure described above whereas at least one crossing should have occurred, as indicated by the fact that the two trajectories had passed through the orientation-reversing part of the Poincaré section. We have therefore modified our algorithm so that two crossings are counted when such intervals were detected. This simple correction yielded the expected results in almost any case. Values of Table 1 for which this has been applied are displayed in square brackets. It should be noted that in many cases, the correct results could also be recovered by decreasing η to $2b_0$, which gives some confidence about the validity of this procedure. However, decreasing η induces spurious crossings for some other pairs of orbits, and a sensible comparison between theoretical and experimental values requires that these latter be obtained from a unique algorithm with fixed parameter η.

Three values in Table 1 are not those predicted by the horseshoe template and are displayed in braces. We have observed that these errors were removed by increasing η to $4b_0$ or $5b_0$, and should therefore be due to spurious crossings.

Self relative rotation rates of orbits up to period $12T$ can be found in Tables 1 and 2, and Table 3 displays knot polynomials of orbits up to period $8T$. Invariants of single orbits seem to be less sensitive to experimental uncertainties than those characterizing pairs of orbits, as self relative rotation rates and knot polynomials computed from the experimental data are in perfect agreement with those predicted from the horseshoe template.

These results strongly support the hypothesis that chaos in the CO_2 laser with modulated losses occurs through the formation of a Smale's horseshoe, one of the simplest mechanisms responsible for chaotic behavior. This result is consistent with previous theoretical investigations [Solari & Gilmore, 1988].

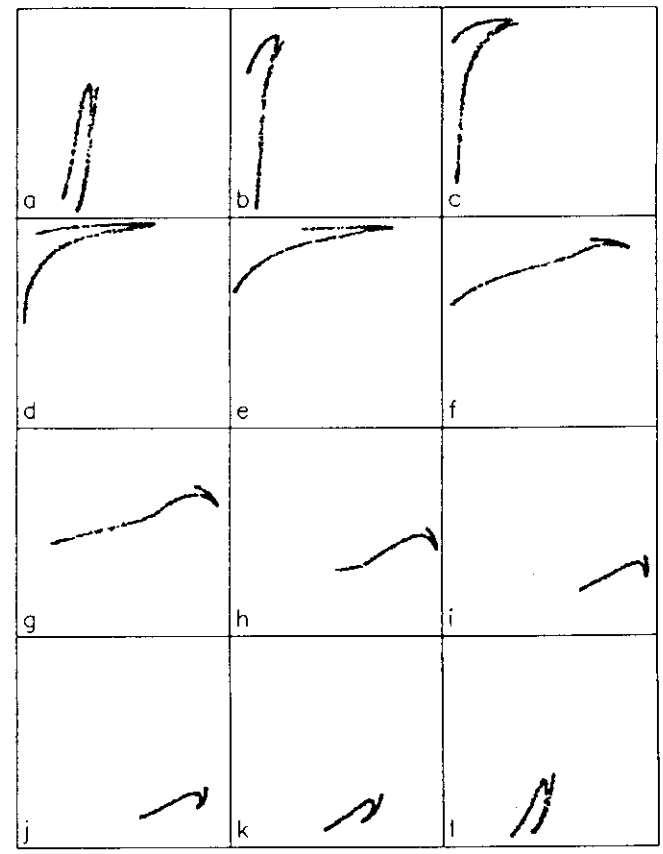

Fig. 7. Poincaré sections of a chaotic attractor in a $\{X(t), X(t+\tau), \phi\}$ phase space with $\tau = T/4$. ϕ increases by $\pi/6$ between consecutive figures.

Table 3. Conway polynomials and knot types of extracted periodic orbits up to period $8T$. $(a_0, a_1, \ldots, a_n)_{2n}$ stands for the polynomial $a_0 + a_1 z^2 + a_2 z^4 + \cdots + a_n z^{2n}$.

Orbits		Conway Polynomial	Knot Type
y	1	1	trivial
xy	2	1	trivial
xy^2	3	1	trivial
xy^3	4	$1 + z^2$	(2, 3) torus
xy^4	5a	$1 + 3z^2 + z^4$	(2, 5) torus
$xyxy^2$	5b	$1 + 3z^2 + z^4$	(2, 5) torus
$xyxy^3$	6a	$1 + 8z^2 + 14z^4 + 7z^6 + z^8$	(3, 5) torus
xy^5	6b	$1 + 8z^2 + 14z^4 + 7z^6 + z^8$	(3, 5) torus
$xyxy^4$	7a	$1 + 16z^2 + 60z^4 + 78z^6 + 44z^8 + 11z^{10} + z^{12}$	(3, 7) torus
xy^6	7b	$1 + 16z^2 + 60z^4 + 78z^6 + 44z^8 + 11z^{10} + z^{12}$	(3, 7) torus
$(xy)^2xy^2$	7c	$1 + 12z^2 + 31z^4 + 27z^6 + 9z^8 + z^{10}$	(7, 3, −2) pretzel
$(xy)^2xy^3$	8a	$(1, 25, 155, 305, 451, 275, 90, 15, 1)_{16}$	{(2, 13); (2, 3)} iterated torus
xy^7	8b	$(1, 30, 235, 741, 1131, 936, 442, 119, 17, 1)_{18}$	(4, 7) torus
$xyxy^5$	8c	$(1, 30, 235, 741, 1131, 936, 442, 119, 17, 1)_{18}$	(4, 7) torus
xy^2xy^4	8d	$(1, 21, 105, 189, 157, 65, 13, 1)_{14}$	(3, 8) torus

The template of a flow describes schematically in which way trajectories on the attractor experience the folding and stretching mechanisms which are responsible for chaotic behavior. When the attractor has a fractal dimension sufficiently close to 2, the template is also easily determined by inspecting the evolution of Poincaré sections at $\phi = \phi_0$ when ϕ_0 is varied from 0 to 2π. This is illustrated in Fig. 7, which shows successive Poincaré sections as ϕ_0 is increased in steps of $\pi/6$. Folding occurs from Fig. 7(f) to Fig. 7(l), where the Poincaré section has the characteristic form of a horseshoe. It can be checked that the left branch of the section in Fig. 7(l) contains trajectories which do not experience rotation between 0 and 2π, indicating that the global torsion of the flow is zero, whereas the right branch corresponds to a torsion of half a turn.

It should be emphasized that topological analysis is complementary to dimension or entropy calculations since it assigns the mechanisms from which chaos originates (e.g., formation of a Smale's horseshoe) in addition to simply proving that the data set is chaotic. It is yet not disconnected from metric measures of chaos, as the first return map of an attractor with an n-branch template has a topological entropy bounded by Log n. This means that the positive Lyapunov exponent λ of our system verifies $\lambda T <$ Log 2.

In conclusion, unstable periodic orbits have been extracted from time series from a CO_2 laser with modulated losses for various values of the control parameters. While knots and links are defined in three-dimensional space only, the topological invariants of periodic orbits could be determined directly from the time series, using only implicitly a three-dimensional embedding. Knowledge of the topological organization of the observed chaotic regimes allowed us to identify, in the range of parameters studied, the template for our system with the Smale's horseshoe template with zero global torsion.

Acknowledgments

We are very much indebted to Francesco Papoff, Ennio Arimondo and Robert Gilmore for enlightening discussions.

References

Arecchi, F. T., Meucci, R., Puccioni, G. P. & Tredicce, J. R. [1982] "Experimental evidence of subharmonic bifurcations, multistability, and turbulence in a *Q*-switched gas laser," *Phys. Rev. Lett.* **49**, 1217.

Birman, J. S. & Williams, R. F. [1983] "Knotted periodic orbits in dynamical systems I: Lorenz's equations," *Topology* **22**, 47.

Birman, J. S. [1975] *Braids, Links and Mapping Class Groups* (Princeton University Press, Princeton).

Dangoisse, D., Glorieux, P. & Hennequin, D. [1987] "Chaos in a CO_2 laser with modulated parameters: Experiments and numerical simulations," *Phys. Rev.* **A36**, 4775.

Grassberger, P. & Procaccia, I. [1983] "Characterization of strange attractors," *Phys. Rev. Lett.* **50**, 346.

Guckenheimer, J. & Holmes, P. [1983] *Nonlinear Oscillations, Dynamical Systems, and Bifurcations of Vector Fields* (Springer-Verlag).

Holmes, P. & Williams, R. F. [1985] "Knotted periodic orbits in suspensions of Smale's horseshoe: Torus knots and bifurcation sequences," *Arch. Rat. Mech. Anal.* **90**, 115.

Holmes, P. [1988] "Knots and orbit genealogies in nonlinear oscillators" in *New Directions in Dynamical Systems*, eds. Bedford, T. & Swift, J. (Cambridge University Press, Cambridge), p. 150.

Kauffman, L. H. [1987] *On Knots* (Princeton University Press, Princeton).

Lefranc, M., Hennequin, D. & Glorieux, P. [1992] "Improved correlation dimension estimates through change of variable," *Phys. Lett.* **A163**, 269.

Lepers, C., Legrand, J. & Glorieux, P. [1991] "Experimental investigation of the collision of Feigenbaum cascades in lasers," *Phys. Rev.* **A43**, 2573.

Midavaine, T., Dangoisse, D. & Glorieux, P. [1985] "Observation of chaos in a frequency-modulated CO_2 laser," *Phys. Rev. Lett.* **55**, 1989.

Mindlin, G. B., Hou, X.-J., Solari, H. G., Gilmore, R. & Tufillaro, N. B. [1990] "Classification of strange attractors by integers," *Phys. Rev. Lett.* **64**, 2350.

Mindlin, G. B., Solari, H. G., Natiello, M. A., Gilmore, R. & Hou, X.-J [1991] "Topological analysis of chaotic time series data from the Belousov–Zhabotinskii reaction," *J. Nonlinear Sci.* **1**, 147.

Oppo, G.-L., Tredicce, J. R. & Narducci, L. M. [1989] "Dynamics of vibro-rotational CO_2 laser transitions in a two-dimensional phase space," *Opt. Commun.* **69**, 393.

Papoff, F., Fioretti, A., Arimondo, E., Mindlin, G. B., Solari, H. & Gilmore, R. [1992] "Structure of chaos in the laser with saturable absorber," *Phys. Rev. Lett.* **68**, 1128.

Solari, H. G. & Gilmore, R. [1988] "Relative rotation rates for driven dynamical systems," *Phys. Rev.* **A37**, 3096.

Tufillaro, N. B., Solari, H. G. & Gilmore, R. [1990] "Relative rotation rates: Fingerprints for strange attractors," *Phys. Rev.* **A41**, 5717.

Tufillaro, N. B., Abbott, T. & Reilly, J. [1992] *An Experimental Approach To Nonlinear Dynamics And Chaos* (Addison-Wesley).

Tufillaro, N. B., Holzner, R., Flepp, L., Brun, E., Finardi, M. & Badii, R. [1991] "Template analysis for a chaotic NMR laser," *Phys. Rev.* **A44**, 4786.